Impact of Backbone Flexibility on the Thermomechanical Property of Semiconducting Polymers with Conjugation Breaker

Luke A. Galuska[α], William W. McNutt[β], Zhiyuan Qian[α], Song Zhang[α], Daniel Weller[α], Sujata Dhakal[α], Eric King[α], Zhiqiang Cao[α], Jason Azoulay[α], Jianguo Mei*[β], Xiaodan Gu[α]*

[α]School of Polymer Science and Engineering, The University of Southern Mississippi, Hattiesburg, MS 39406, USA

[β]Department of Chemistry, Purdue University, West Lafayette, IN 47907, USA

ABSTRACT: Recent reports have shown increased interest in the capacity of conjugation break spacers (CBS) to soften relatively rod-like conjugated polymers (CP) to yield low moduli, high ductility, all while maintaining charge mobility in conjugated polymer blends. Despite this increased interest there remains a lack of fundamental understanding in the role of CBS on backbone rigidity of conjugated polymers and their thermomechanical properties. Here, we provide a first holistic approach to understand the fundamental influence of CBS length on an n-type naphthalene diimide-based conjugated polymer, denoted by PNDI-Cx. CBS lengths are varied from C0 (fully conjugated) to C7 with the CBS engineered into each repeat unit for systematic evaluation. Solution small angle neutron scattering (SANS) and oscillatory shear rheometry were employed to provide the first quantitative evidence of CBS influence over conjugated polymer chain rigidity and entanglement molecular weight (M_e), demonstrating a reduction in Kuhn length from 521 Å to 36 Å for fully conjugated PNDI-C0 and PNDI-C6, respectively, as well as a nearly consistent M_e of ~ 15 kDa upon addition of CBS. Thermomechanical properties, including: elastic modulus, glass transition temperature, and melting temperature were all shown to decrease with increasing CBS length. An extraordinary ductility, upwards of 400% tensile stain before fracture, was observed for high molecular weight PNDI-C4 which we attribute to a high number of entanglements and disruption of crystallization. Furthermore, the deformation mechanism for PNDI-Cx was studied under strain through X-ray diffraction, polarized UV-vis, and atomic force microscopy.

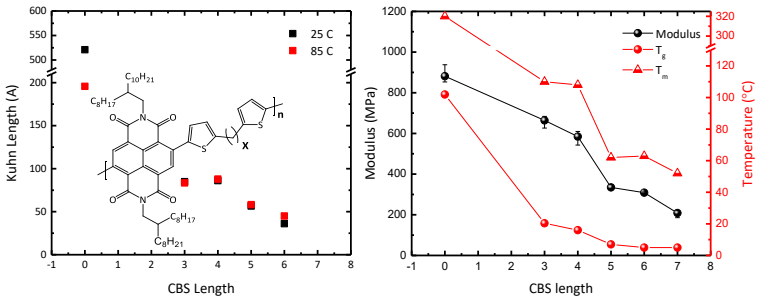

Introduction

A main attribute of organic semiconductors is the potential to produce inherently soft and ductile electronics for emerging applications in technology such as wearable and implantable devices.[1,2,3] Such applications require an active material with high charge transport and compliance similar to biological tissue. Conjugated polymers (CPs) have seen vast improvements in charge transport performance in the last three decades[4], this improvement has driven recent research interest towards the investigation of mechanical performance which is still in its infancy. Key parameters governing the mechanical property include: glass transition temperature (T_g), entanglement molecular weight (M_e), and morphology which are all highly dependent on the chemical structure and specifically chain flexibility. Despite the high heterogeneity of many CPs, the structural components can be separated into two regions of interest, namely, side chains which offer enhanced solubility and a conjugated backbone which promotes charge transport. Side-chain engineering offers a reliable route for tuning the mechanics through moderate influence over backbone chain dynamics. Increasing side chain length promotes plasticization of the backbone resulting in a reduction in T_g and subsequently the modulus, which has been previously demonstrated with poly(3-alkylthiophenes) (P3AT).[5,6] More recently, Sugiyama et al. investigated the influence of side-chain length, branching, and chemical structure on a diketopyrrolopyrrole (DPP) based D-A polymer, concluding that increased length and flexibility of the side-chain will result in reduced T_g and increased ductility.[7] Although a successful method for tuning the modulus, side-chain engineering is relatively indirect compared to direct modification of the polymer backbone.

Backbone engineering provides a more direct control over chain flexibility which is a key contributing factor to backbone T_g as well as the propensity of chains to entangle which governs ductility. Solution scattering is the principal route to quantitatively assess chain flexibility, but has primarily been limited to more conventional CPs such as P3ATs[8,9,10],polyfluorene (PF)[11], and poly(p-phenylene vinylene) (PPV)[12]. The general consensus is that CPs containing higher content of fused rings will have greater rigidity due to an increase in the rotational energy barrier thus reducing conformational freedom.[13] This is evident in the comparison of P3HT and fused PF which exhibit a persistence length of approximately 3 nm[10] and 7 nm[11] respectively. Previous research by Roth et al. explored a broad library of 51 low-bandgap polymers of varying architecture, demonstrating that a higher content of fused rings to result in increased stiffness as well as likelihood of fracture.[14] A similar trend was

observed in our recent publication where we examined the effect of isolated and fused thiophene content on the thermomechanics of DPP-based polymer.[15] It was discovered that increasing thiophene content exhibited an anti-plasticization effect yielding an increase in modulus and reduced ductility.

Conjugation break spacers (CBS) were recently introduced to the field of organic electronics in 2014 by Sivula to disentangle the effect of intra and intermolecular transport.[16] For randomly incorporated CBS at small concentration, the charge mobility was found to be largely maintained relative to the parent PBTTT polymer. Although no mechanical properties were considered, this study has sparked interest in the conjugated polymer community for utilizing flexible CBS to reduce backbone rigidity and enhance mechanical performance without compromising charge mobility. The first mechanical study of such systems was performed by Savagatrup et al. in 2016, in which the effect of CBS concentration on a DPP-based polymer was investigated.[17] A reduction in modulus was found upon increasing CBS content. Despite the supposed increase in flexibility offered by incorporation of CBS the strain at failure was observed to be surprisingly low, below 15% strain, regardless of CBS content. This was justified through the solid-state packing, where alkyl packing distance and full width half max (FWHM) decreased with increasing CBS, indicating that morphology and not structure alone are responsible for the deformation mechanics within these systems. Also, in 2016, Savagatrup et al. investigated the influence of CBS length upon incorporation into the monomer repeat unit itself where previously only random copolymers have been reported.[18] Although, the thermomechanics of these systems were not considered, a surprisingly high charge mobility was maintained for blend systems containing as little as 2% fully conjugated DPP within a matrix of CBS based polymer. Many more investigations on the utilization of CBS have been reported, including: promotion of solubility and melt processability[19,20,21,22], healable semiconductors[23], and semi-random copolymers.[24,25] However, there remains a fundamental gap in knowledge for these systems, namely a lack of quantitative information regarding the influence of CBS on chain rigidity, propensity to entangle, and mechanical dependence on molecular weight.

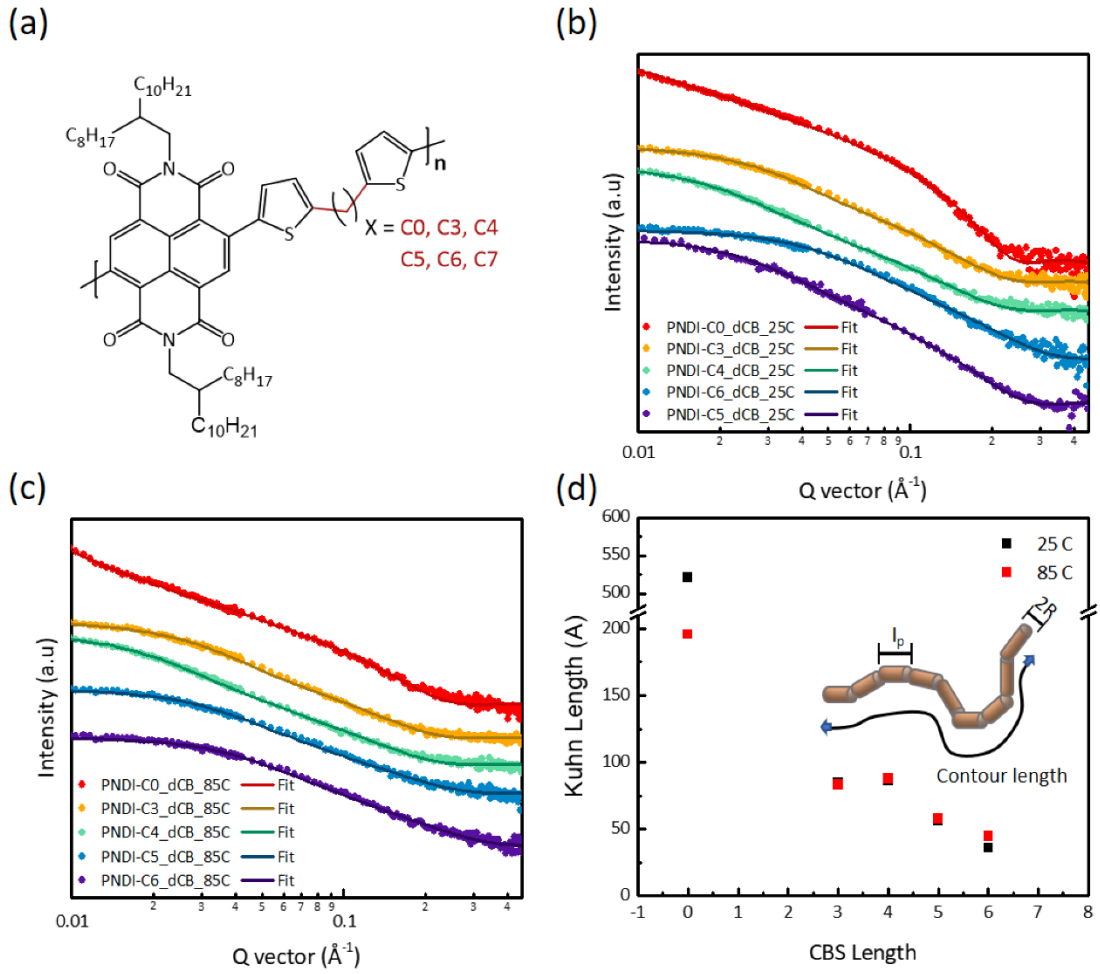

Figure 1: Solution SANS profile and fitting of (a) PNDI-Cx polymers in d-DCB solvent at (b) 25 ˚C and (c) 85 ˚C. (d) Kuhn length dependence on CBS length as fitted using the flexible cylinder model in SasView software.

Here, we investigate NDI-based polymer as the first n-type polymer to be incorporated with CBS of varying length to ascertain the role of backbone flexibility on thermomechanics as well as morphology. Our findings provide a quantitative verification that increased backbone flexibility results in a softening effect expressed through a reduction in T_g and elastic modulus.

An extremely high ductility, upwards of 400% strain, is observed at multiple CBS lengths and determined to be directly proportional to the number of entanglements in the system given by oscillatory melt shear rheology and molecular weight dependent mechanical analysis using our unique film on water tensile tester. Given the profound ductility, a high degree of alignment was observed and characterized through an in-depth morphological analysis, including grazing incidence wide angle X-ray scattering (GIWAXS), transmission WAXS, polarized UV-Vis, and atomic force microscopy (AFM).

Results and Discussion

Chain rigidity characterization using solution small angle neutron scattering. NDI-based conjugated polymer was utilized to investigate the effect of CBS length on backbone flexibility with the CBS incorporated into each repeat unit for systematic evaluation (**Figure 1a**). Random incorporation of CBS masks the inherent influence over both electrical and thermomechanical performance due to two factors: 1) While CBS concentration can be relatively maintained, its placement within the polymer structure is unclear and may provide varying effects at the chain end or centrally located along the backbone. This becomes particularly important for low molecular weight polymer systems where it's feasible to consider that only one CBS may be incorporated into the polymer chain. 2) Packing morphology is greatly affected by structure consistency and upon random insertion, disruption of the morphology is likely to occur and act as defects towards crystallization.[26,27,28] Therefore, the properties obtained from such systems may be dominated by the morphology induced from random addition rather than the CBS itself. Thus, this work opted to investigate 100% incorporation of the CBS to elucidate the effect of backbone flexibility on thermomechanical property.

The CBS length was varied from C0 (fully conjugated) to C7 with the purpose of demonstrating the effect of increasing backbone flexibility on the thermomechanics. Despite the notion that CBS offers improved flexibility for conjugated systems, there is currently no quantitative experimental evidence of this in the literature. In order to investigate the polymer chain conformation, solution small angle neutron scattering (SANS) was conducted for each polymer (2D scattering profiles are available in **Figure S1** in the supplemental information). A 5 mg/ml concentration in deuterated dichlorobenzene was used to provide a strong coherent scattering signal while also being sufficiently dilute to obtain non-interacting polymer chains and thus elucidating the form factor. Temperature was also controlled at both 25 ˚C and 85 ˚C to consider variable solvent interactions as well as potential aggregation of conjugated polymer, especially for fully conjugated PNDI-C0. The scattering data was fitted to the flexible cylinder model in SasView[29] software which enabled the calculation of the chain rigidity through the Kuhn length (L_k) (**Figures 1b-d** and **Table S1**). The L_k was shown to dramatically diminish upon insertion of C3 CBS from 521 to 85 Å in the case of 25 ˚C and 196 to 84 Å for 85 ˚C. Such strong temperature dependence is only found in PNDI-C0 which may indicate a transition to a more disaggregated state, while all CBS containing PNDI-Cx polymers are highly soluble and interact strongly with the solvent at room temperature. Upon further increasing the CBS length, the L_k continued to reduce indicative of increased flexibility, thus providing the first experimental evidence that incorporation of CBS does indeed increase the flexibility within conjugated systems.

Thermomechanical property. An in-depth thermomechanical analysis was performed to ascertain the impact of chain flexibility, provided by the CBS, on glass transition temperature (T_g), elastic modulus, and crack-onset strain (COS). Such parameters ultimately govern the softness and ductility that can be achieved for intrinsically stretchable electronics. In past literature, differential scanning calorimetry (DSC) has shown to be unreliable for the characterization of glass transition phenomena associated with conjugated polymer. This is due to high backbone rigidity, semi-crystalline nature, and high side chain content which ultimately results in a low backbone Δc_p that is nearly imperceptible when using conventional DSC.[30,31] In the case of PNDI-C0, physical aging was used in our previous publication to elucidate the T_g through the associated enthalpy overshoot and further verified with a modified DMA technique.[30,32] The resulting values previously obtained for PNDI-C0 were 101 and 131 ˚C respectively. In contrast, the enhanced backbone flexibility and reduced crystallinity of PNDI-Cx polymers containing CBS provide a strong T_g signal from conventional DSC. Glass transition was studied with DSC at a heating/cooling rate of 30 ˚C/min, the thermograms are shown in **Figure S2**. **Figure 2a** reveals a clear reduction in both T_g and melting temperature (T_m) with increasing CBS length. This demonstrates a strong dependence of backbone flexibility to influence chain dynamics and crystalline packing. The most dramatic change occurs upon introduction of the CBS unit where backbone flexibility is dramatically enhanced due to the break in conjugation. While addition of CBS with greater length provides diminishing improvement in flexibility and T_g as chain dynamics are already quite mobile.

From the thermal analysis we hypothesized a reduction in the elastic modulus with increasing CBS length due to greater chain dynamics as expressed by the reduction in T_g. This was verified through the use of the pseudo-free-standing tensile tester which as described in our previous publications enables the mechanical property of an ultrathin film to be directly obtained through stress-strain analysis while supported by a smooth water surface.[15,33,34,35,36] Prior to characterization, each polymer film was annealed under a nitrogen atmosphere for two days at either the

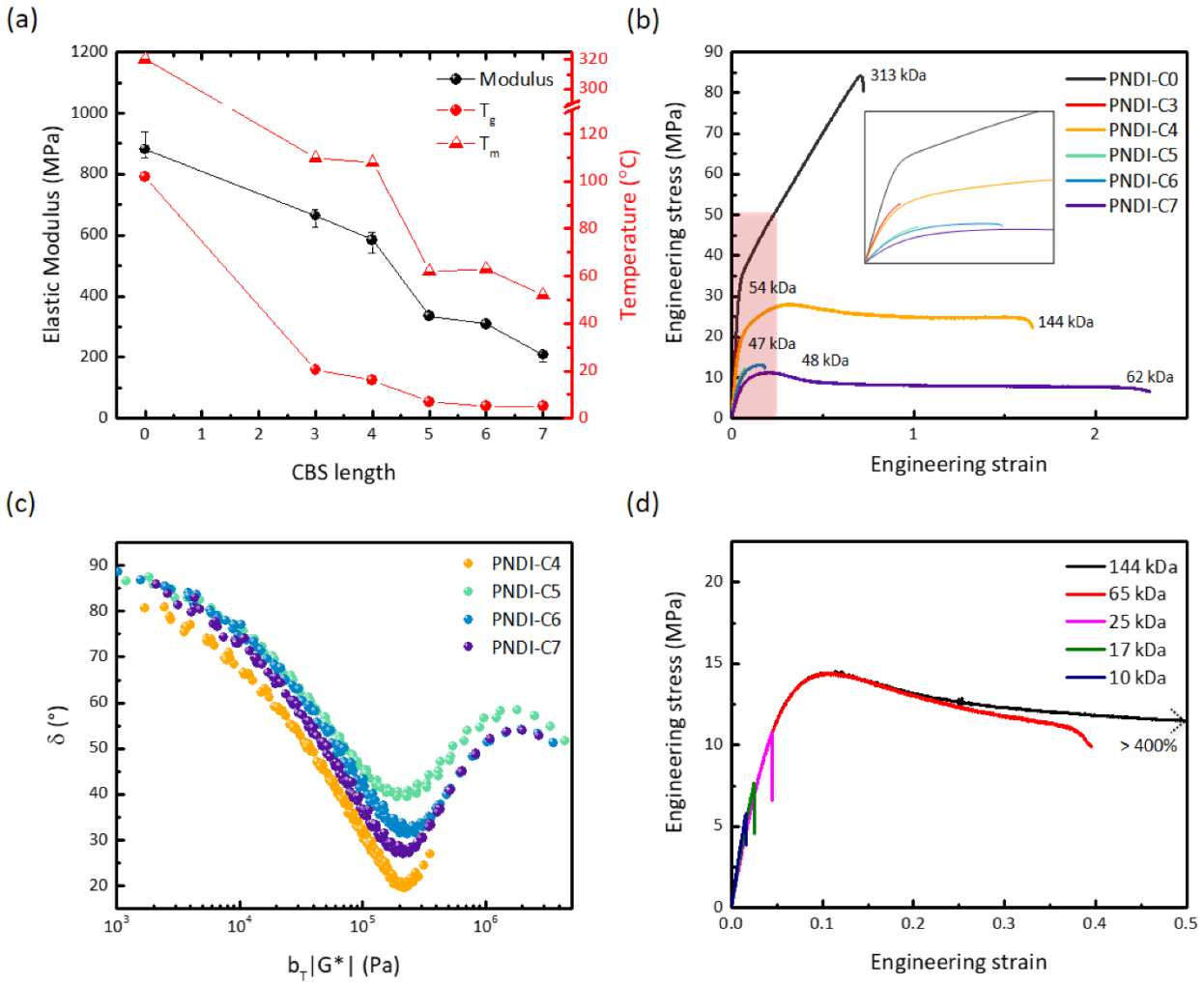

Figure 2: Influence of chain flexibility on thermomechanical and rheological property. (a) Elastic modulus, backbone T_g, and T_m for all examined PNDI-Cx polymers. Thermal data was obtained from DSC and T_g was verified through physical aging. (b) Comparison of stress-strain curves obtained from the pseudo-free-standing tensile test post a two-day annealing at an undercooling of ~ 30 ˚C. PNDI-C0 was annealed for 8 hours at 200 ˚C. Shaded red area indicates region of interest relative to insert. (c) Molecular weight dependent tensile test of PNDI-C4 post two-day equilibrating at room temperature in nitrogen atmosphere. (d) Van Gurp-Palmen-plots of PNDI-C4 - C7.

operating temperature of the tensile tester (25 ˚C) or an undercooling of 30 ˚C below each polymer's respective T_m. The rationale for this is two-fold: 1) The thermal properties of the PNDI-Cx polymers, namely $T_g < T_{operating} < T_m$, allow for isothermal crystallization to take place at room temperature which may yield time-dependent mechanics as the morphology is in a state of flux. 2) The increased flexibility of these systems yields relatively slow crystallization rates as compared to the fully conjugated PNDI-C0, whose crystallization cannot be impeded even when cooling from the melt at rates of more than 10,000 K/s.[30] Thus, the annealing protocol was designed to achieve equilibrated morphologies for deriving structure-property relationships without the obfuscation of time dependence. **Figure 2b** shows representative curves for the tensile analysis at 30 ˚C undercooling (see **Figure S3** for raw curves) where a clear trend in elastic modulus is given by the diminishing slope in the linear elastic regime thus confirming our hypothesis. However, it is important to note that in the case of PNDI-Cx films annealed at room temperature the trend in modulus is not as clear, which may be due to the variable thermodynamic driving force towards crystallization. A summary of the tensile data from both regimes is given in **Table 1**. The COS for the polymers covers a wide range from below 5% strain to above 400% in the case of high molecular weight PNDI-C4 annealed at 25 ˚C.

Stretchability or COS is often found to be proportional to the number of intermolecular entanglements in a polymer system.[37,38,39] As the number of entanglements increase, the distribution of load bearing chains becomes more uniform minimizing the influence of inherent defects and ultimately providing increased elasticity. Due to limited material supply, the sample was molded into disks 8 mm in diameter and 0.5 mm in thickness under vacuum for oscillatory melt shear rheology.[40,41,42,43] The rheological measurements were successful for PNDI-C4 to C7 and the associated master curves are given in **Figure S4**.

Table 1: Physical and mechanical properties of NDI-Cx polymers

	M_n (kDa)	M_w (kDa)	PDI	Me (kDa)	Thickness (nm)	Modulus (Mpa)	STDEV	COS	STDEV
PNDI-C0	157.5	313.4	2.0	---	97	691	38	0.69	0.05
PNDI-C0 PA	157.5	313.4	2.0	---	115	881	26	0.65	0.11
PNDI-C3	33.2	53.9	1.6	---	83	293	3	0.83	0.53
PNDI-C3 PA	33.2	53.9	1.6	---	135	664	19	0.04	0.01
PNDI-C4	4.73	9.6	2.0	---	67	386	25	less than 0.02	NA
PNDI-C4	10.5	17.3	1.6	---	71	364	6	0.03	0.01
PNDI-C4	14.6	24.6	1.7	---	82	320	8	0.04	0.01
PNDI-C4	34.1	64.8	1.9	---	94	312	16	0.43	0.18
PNDI-C4	61.3	144.3	2.4	15.9	78	338	11	4.04	0.27
PNDI-C4 PA	61.3	144.3	2.4	15.9	66	585	25	1.10	0.55
PNDI-C5	15.3	46.5	3.0	15.9	83	335	10	0.06	0.01
PNDI-C6	16.7	48.0	2.9	14.2	99	309	3	0.16	0.02
PNDI-C7	19.0	62.3	3.3	14.8	79	213	7	1.80	0.41

PA: post annealing at 30 ˚C below the respective melting temperature

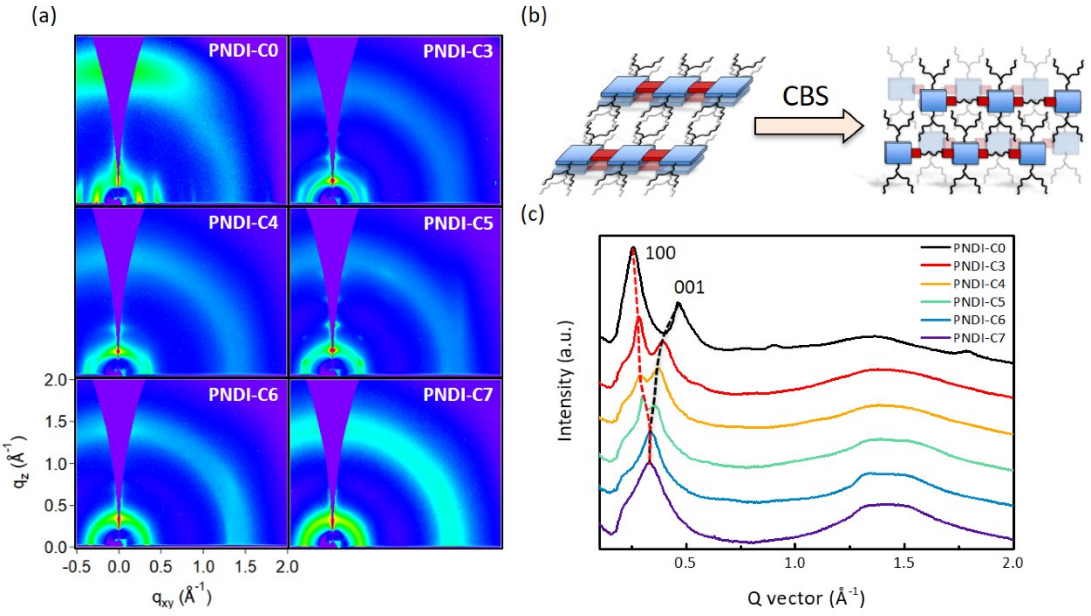

Figure 3: (a) 2D GIWAXS profiles of as cast NDI-Cx films. (b) Schematic diagram of the shifting solid-state morphology upon addition of CBS. Face-on PNDI-C0 with strong pi-pi stacking transforms to predominantly edge-on PNDI-Cx with disordered pi-pi stacking and closer alkyl packing. (c) 1D in-plane line cut profile.

Van Gurp-Palmen-plots (vGP-plot) were constructed to elucidate the entanglement characteristics, namely the entanglement molecular weight (M_e) and the degree of entanglement (**Figure 2c**).[44,45,46] The entanglement plateau modulus G_N was obtained from the norm of complex modulus corresponding to the minimum phase angle of the vGP-plot. G_N is shown to be rather independent of CBS length with values ranging indiscriminately from 19-23 kPa. This also implies a consistent M_e through the equation:[47]

$$G_N = \frac{\rho RT}{M_e} \qquad \text{eq1}$$

which is in the range of 14-16 kDa. Additionally, the position of the minimum in respect to the phase angle describes the molecular weight of the system where higher molecular weight polymer is expressed through a lower phase angle. Considering the relatively consistent M_e, the phase angle will be directly related to the number of entanglements within the system and therefore greatest ductility should be found at the minimum phase angle. This was found to be the case as 144 kDa PNDI-C4 possesses the lowest phase angle followed by C7, C6, and C5 which corresponds well to their relative COS of 400%, 180%, 16%, and 6%.

We then performed molecular weight dependent mechanical analysis on PNDI-C4 (**Figure 2d**) with weight average molecular weight (M_w) ranging from 9.6 kDa (just over half M_e) to 144.3 kDa (equivalent to ~ 9 entanglements). Samples with M_w equivalent to 4*M_e were shown to be relatively ductile with above 40% strain at failure, but not to the extent of 144 kDa M_n which could tolerate strains above 400%. This transition is justified given that multiple entanglements are generally required for high ductility. Additionally, given that mechanical analysis was performed on solution cast films the solid-state entanglements cannot be directly understood as the M_w to entangle is greater for solution than the melt state at which rheometry was performed. Regardless, we highlight the importance of obtaining material properties such as M_e which has a profound influence over both mechanical and electrical property yet has generally been overlooked.

Morphology. Next, grazing incidence wide angle X-ray scattering (GIWAXS) was used to study the film crystalline morphology (**Figure 3 and Table S2**). PNDI-C0 has predominantly face-on morphology with strong π-π stacking as well as in-plane (100) and (001) scattering peaks corresponding to the alkyl and backbone respectively, consistent with literature.[48,49] Upon addition of CBS we observed a shift from the face-on to edge-on morphology as well as a significant loss of π-π stacking. Additionally, the in-plane q vector of the (100) peak was shown to increase from 0.258 to 0.337 $Å^{-1}$ indicating a more closely packed alkyl system and the (001) peak was shown to decrease from 0.470 to 0.332 $Å^{-1}$ indicative of increasing CBS length which provides the contrast to elucidate the (001) peak.

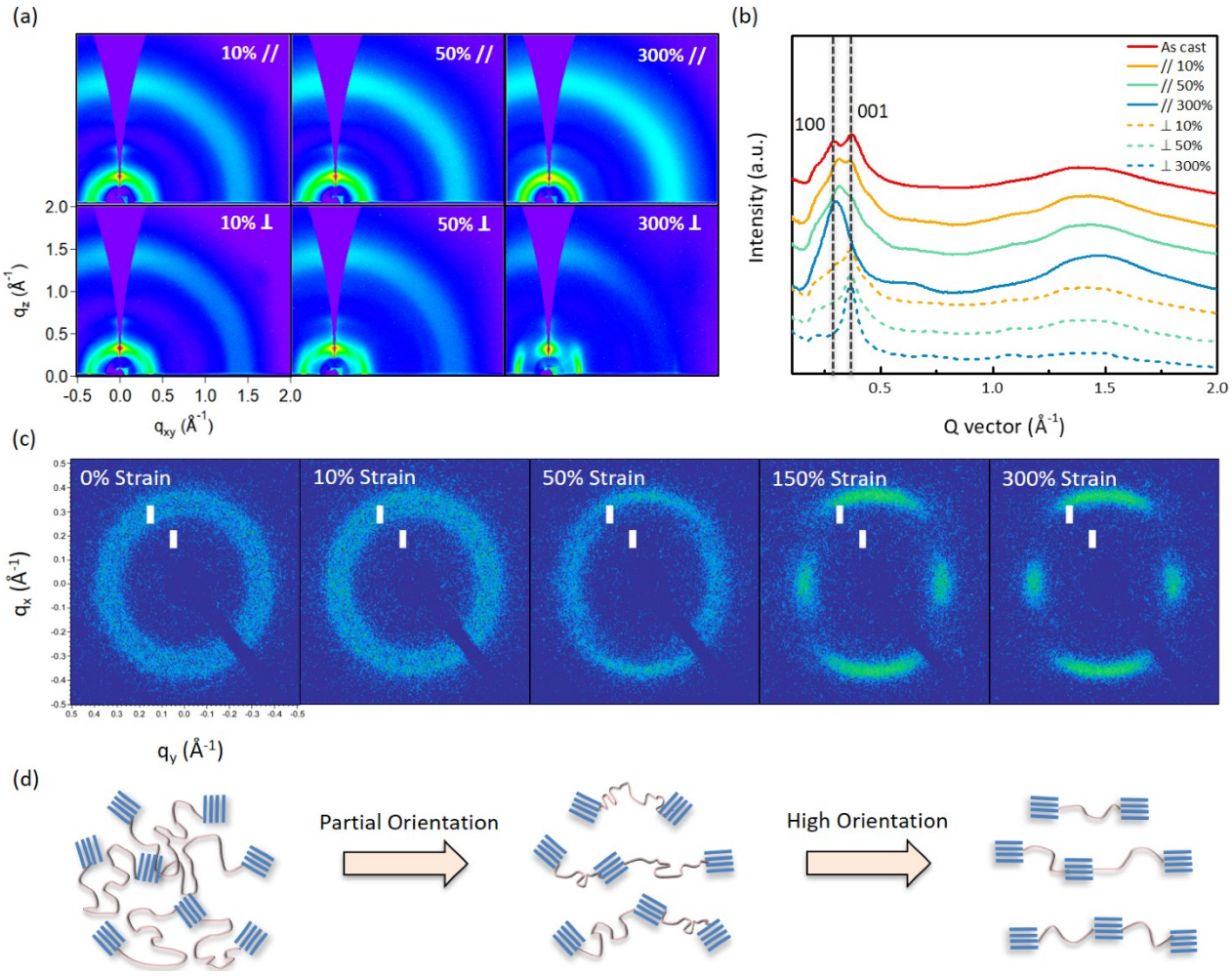

Figure 4: X-ray characterization for deformed PNDI-C4 polymer. (a) 2D GIWAXS profile of PNDI-C4 under tensile strain for both parallel and perpendicular exposures relative to strain direction. (b) 1D in-plane line cut scattering profile. (c) 2D transmission WAXS profiles of free-standing thin film (192-119 nm thickness) PNDI-C4 under ex-situ tensile strain. (d) Diagram showing an increase in orientation corresponding to transmission WAXS at 0, 50 and 300% strain.

This trend continues until a CBS length of C6 is reached at which point the alkyl and backbone scattering become indistinguishable.

Deformation mechanism and tensile alignment of polymer backbone. X-ray scattering technique was extensively used to determine the degree of alignment in the crystalline region for PNDI-Cx. GIWAXS was performed on tensile strained PNDI-C0, C3, C4, and C7 to study the effect of tensile alignment on these ductile systems (**Figure 4a**, **Figures S6-S7** and **Table S3**). The d-spacing of (100) and (001) were largely maintained upon strain and a shift in the orientation of these scattering peaks was evident through comparison of perpendicular and parallel exposures to the strain direction. PNDI-C4 showed the most dramatic alignment, evident in **Figure 4b**, where an increase in the (100) intensity occurred with increasing strain along with a reduction in the (001) intensity for exposure parallel to strain. The opposite trend occurs for exposure perpendicular to strain where the (001) scattering is the majority of the detected signal. Such scattering is indicative of a highly aligned system. Unfortunately, the illuminated volume was not well accounted for, thus preventing accurate normalization and quantitative understanding of the alignment. To quantify the degree of alignment we transitioned towards ex-situ transmission circle gathering analysis (**Figure 5a-b**) the peak area was determined to increase with strain up to 150% upon which the area decays towards 300% strain. This was observed for both (100) and (001) although we note the trend is inconsistent in the case of (100). The FWMH of (001) peak was determined to decrease with increasing strain (**Table S4-S5**). Together the increase in area and reduction in FWHM imply an increased backbone contribution and a greater long-range order pervading throughout the system. Pole figure analysis was performed for both (100) and (001) scattering peaks to assess the contribution of scattering at each azimuthal angle and analyzed using Walker/Wagner alignment factor methodology to quantitatively determine the degree of tensile induced alignment (**Figure 5c-d**).[50] We note a high degree of alignment upwards of 0.3 and -0.5 for (100) and (001) regimes respectively which plateaus post 150% strain; this is in agreement with both observed area and FWHM trends. A value of 1 or -1 represents a purely aligned system orientated in the horizontal and vertical directions respectively and agrees with (100) and (001) orientation direction. For plotting purposes, the absolute value of the alignment factor was taken, as the direction of orientation is inconsequential for quantitative confirmation of alignment.

While the discussed above X-ray technique only probes the

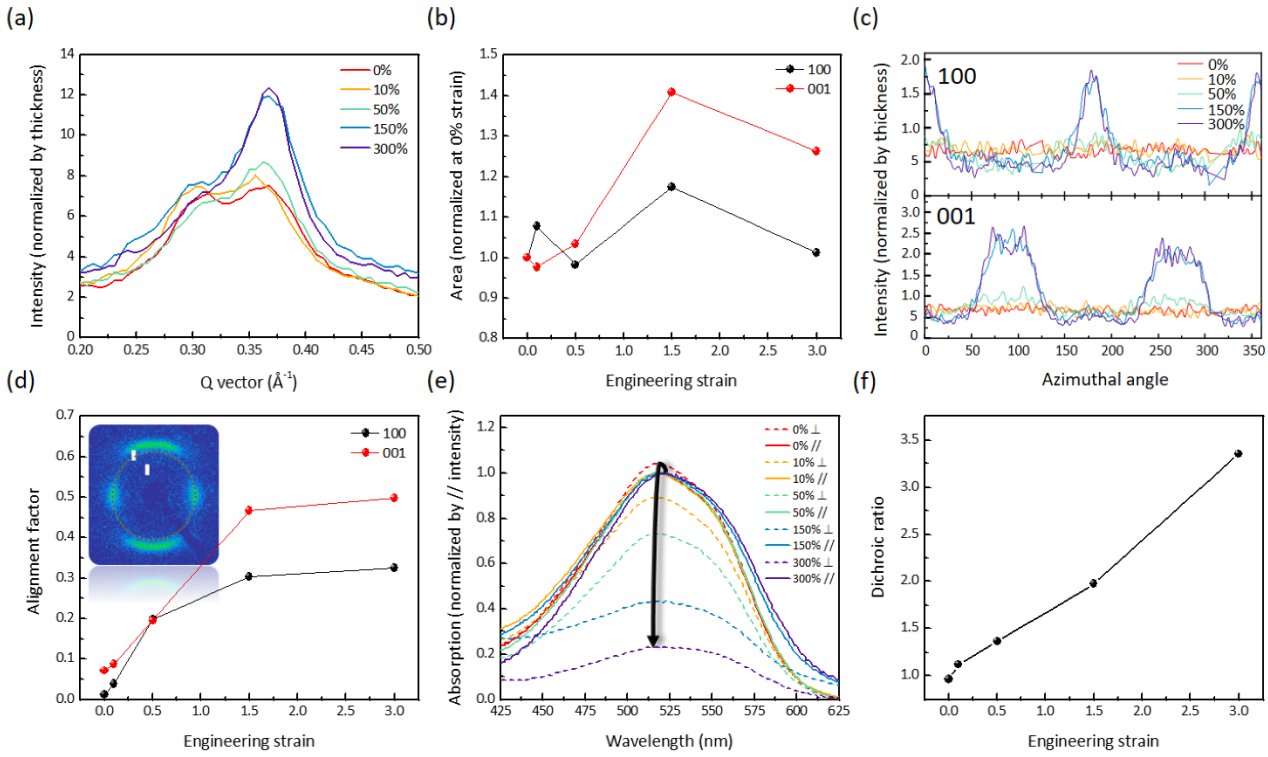

Figure 5: Alignment analysis of NDI-C4 under tensile strain. (a) 1D circle gathering plot obtained from transmission WAXS and (b) fitted peak area. (c) Pole figure analysis of 100 and 001 peaks at q vectors of 0.305 and 0.366 Å^{-1} respectively and (d) resulting alignment factor analysis. (e) Polarized UV-Vis parallel and perpendicular to strain normalized by the absorption in the parallel to strain direction and (f) the corresponding dichroic ratio.

WAXS which provides enhanced elucidation of the in-plane morphology which encompasses the (100) and (001) peaks of interest. The transmission 2D profiles are given in **Figure 4c** and were achieved for free standing films with thickness ranging from 192 to 120 nm depending on extent of strain. Through crystalline regions, the alignment of amorphous domains must also be considered. To confirm the highly aligned system of PNDI-C4 we then performed polarized UV-Vis (**Figure 5e-f**) to study the whole chain align (both amorphous and crystalline) as well as atomic force microscopy (AFM) (**Figure S8**) for

topographical investigation. Polarized UV-Vis is unique for conjugated polymers as the transition dipole moment (π-π*) lies parallel to the backbone thus enabling elucidation of alignment through comparison of parallel and perpendicular absorption intensities, also known as the dichroic ratio.[51] This is demonstrated in **Figure 5e** where the parallel to strain absorption is normalized for each strain and we note the perpendicular to strain absorption diminishes with increasing strain. This correlates to a linearly increasing dichroic ratio up to a value of 3.35 in the case of 300% strain. Furthermore, it is feasible to expect an even greater dichroic ratio throughout the tensile process as PNDI-C4 possess a T_g below room temperature, thus significant relaxation of amorphous domains is expected prior to measurement. Together with transmission WAXS, this indicates an alignment of the crystalline phase followed by plateau and disruption of crystallites at high strain while amorphous domains continue to align given their high chain mobility and degree of entanglement. Although more qualitative, AFM does show an aligned morphology at 300% strain. Considering the high amorphous content in the PNDI-C4 system, it stands to reason that at relatively low strains the relaxation of the surface would prevent significant visual alignment.

Conclusion

In summary, a suite of characterization methodologies was performed on PNDI-Cx polymers to provide a holistic perspective into the role of backbone flexibility on thin film thermomechanics and morphology. For the first time, backbone flexibility was quantitatively shown to significantly reduce upon addition of CBS into the conjugated backbone. Such increase in flexibility was evident through the T_g, T_m and modulus which all demonstrated a reduction with increasing CBS length. A high ductility was observed for high molecular weight PNDI-C4 which was rationalized through the large number of entanglements expressed by oscillating melt-shear rheology. The M_e was discovered to be relatively independent of CBS length and therefore ductility was directly proportional to the molecular weight. In-depth morphological analysis was conducted indicating strong in-plane scattering which was exploited to evaluate the degree of tensile alignment for PNDI-C4. Currently, we are exploring blend mechanics and the possibility of coalignment with a fully conjugated tie-chain as well as the crystallization kinetics of these polymers which was noted in this work to have a strong influence over thin film mechanics.

Methods

Materials and Processing: Six PNDI-Cx polymers were synthesized with CBS units incorporated into each monomer repeat unit. The synthesis was performed as previously described by McNutt et al. For GPC analysis, the polymers were dissolved by shaking in 1,2,4-trichlorobenzene (TCB) at a concentration of 1-2 mg/mL for 2 hrs at 160°C through use of an Agilent PL-SP 260VS sample preparation system, the samples were then filtered through a 2 μm stainless steel filter into the 2 mL glass GPC vials and ran in the instrument at 160°C using TCB as an eluent. The high temp (HT)-GPC utilized was an Agilent PL-GPC-220 system, this system is equipped with 3 pLGel Olexis (13 μm particle size) in series in addition to a differential refractive index (RI) detector, a dual angle (15° and 90°) light scattering (LS) detector, and a viscometer (VS) detector. The chromatograms were worked up from the RI signal utilizing a narrow standard polystyrene calibration (14 points, ranging from 162 g/mol to 3,242,000 g/mol).

PNDI-Cx polymers were dissolved in chlorobenzene at 80 ˚C at a concentration of approximately 25 mg/ml. PNDI-C0 was prepared at 10 mg/ml under identical conditions. Poly(sodium 4-styrenesulfonate) (PSS) was obtained from Sigma Aldrich at a molecular weight of 70 kDa in 30% by volume aqueous solution. PSS was first diluted to 3 wt% in aqueous solution and spun cast onto plasma treated silicon wafer at 4000 rpm for 2 minutes. PNDI-Cx solution was then cast at 2000 rpm for 1 minute forming the composite film.

Solution small angle neutron scattering: SANS was performed at the National Institute of Science and Technology at the NGB 30 m SANS. A wavelength of xxx was used for two sample-detector distances of 1 and 8 m which was combined for increased q vector range. Solution was prepared in deuterated chlorobenzene at 5 mg/ml. Each sample was exposed at both 25 and 85 ˚C with an exposure time of 5 and 30 minutes for sample to detector distances of 1 and 8 m respectively. Data reduction was performed through Wavemetrics Igor. Finally, SasView software was used to fit the scattering data to the flexible cylinder model[52] to calculate the chain rigidity.

DSC: DSC was performed with a Mettler Toledo DSC 3+ at heating and cooling rates of 30 ˚C/min.

Pseudo-free-standing tensile test: Thin film tensile tests were performed on a water surface through the pseudo-free-standing tensile tester, as described in our previous publication.[33] Briefly speaking, the composite films were patterned into a dog-bone geometry using a Boss FM series laser. Laser parameters are as follows: 1064 nm wavelength, 14% power, 80 Hz frequency, and 400 mm/s etching speed. Post patterning, the composite film was floated on top of water before being further unidirectionally pulled at a strain rate of 5×10^{-4} s^{-1} until the film fractures. Generally, five independent samples were measured for each conjugated polymer to provide statistically averaged mechanical properties. The elastic modulus was obtained from the slope of the linear fit of the stress–strain curve within the first 0.5% strain.

Oscillatory melt-shear rheometry: Linear rheological measurements of PNDI-C4 to C7 were performed with strain-controlled rheometer Advanced Rheometric Expansion System (ARES-LS) from TA Instruments under dry nitrogen protection. The sample was molded into a 0.5 mm thick bubble-free disk with 8 mm in diameter under vacuum at 30 °C above the relevant melting temperature. The sample was loaded between 8-mm aluminum disposable parallel plates and heated above the melting temperature to ensure good contacts between sample and plates. The dynamic frequency sweep between 100 to 0.1 rad/s were performed in a wide temperature range: 150 °C to 70 °C for C4, 80 °C to 30 °C for C5, and 100 °C to 30 °C for C6 and C7, after the linear viscoelastic strain range was determined with strain sweep measurements.

GIWAXS: GIWAXS was performed on beamline 11–3 at the Stanford Synchrotron Radiation Lightsource. Data was collected at a sample to detector distance of ~ 300 mm under a helium environment with an incident beam energy of 12.7 keV and an incidence angle of 0.12°. Diffraction analysis was performed using Nika software package within Wavemetrics Igor, in combination with WAXS tools.

Transmission WAXS: Transmission WAXS was performed using a Xenocs Xeuss 2.0 SAXS/WAXS lab source instrument. Free-standing films were exposed for 2.5 hours with an incident beam energy of 8.05 keV and a beam geometry of 1.2 x 1.2 mm. The sample to detector distance was approximately 157 mm. Free-standing films were obtained by lifting post tensile drawn films from the pseudo free-standing tensile tester's water bath using a steel washer with an inner diameter of 3.85 mm. The films were allowed to dry under vacuum at room temperature overnight prior to the obtained scattering. Film thickness was obtained by interferometry and AFM for normalization of the scattering intensity.

Transmission UV-Vis: UV–Vis–NIR transmission spectra were performed with an Agilent Cary 5000 with a specified operating wavelength range of 300 – 1100 nm. Polarized measurements were achieved with a Harrick Glan-Taylor polarizer at 0˚ and 90˚. For tensile drawn samples, measurement was conducted on glass slides after collection and subsequent drying.

AFM: AFM images were acquired on an Asylum Research Cypher S operating in AC mode in air. The samples were collected post tensile strain onto bare silicon wafer.

ASSOCIATED CONTENT

Supporting information is available on-line through the Wiley Online Library or from the author.

Additional figures and tables as described in the text (PDF)

AUTHOR INFORMATION

Corresponding Author

* Email: xiaodan.gu@usm.edu

Author Contributions

The manuscript was written through contributions of all authors. All authors have given approval to the final version of the manuscript.

ACKNOWLEDGMENT

We thank the financial support from U.S. Department of Energy, Office of Science, Office of Basic Energy Science under award number of DE-SC0019361. We also thank the financial support from NSF Office of Integrative Activities #1757220. This work is supported by National Science Foundation Division of Graduate Education (DGE) #1449999. Use of the Stanford Synchrotron Radiation Lightsource, SLAC National Accelerator Laboratory, is supported by the U.S. Department of Energy, Office of Science, Office of Basic Energy Sciences under Contract No. DE-AC02-76SF00515. A portion of this research used resources at the Spallation Neutron Source, a DOE Office of Science User Facility operated by the Oak Ridge National Laboratory. Access to NGB 30 m SANS was provided by the Center for High Resolution Neutron Scattering, a partnership between the National Institute of Standards and Technology and the National Science Foundation under Agreement No. DMR-1508249. This work benefited from the use of the SasView application, originally developed under NSF award DMR-0520547. SasView contains code developed with funding from the European Union's Horizon 2020 research and innovation programmed under the SINE 2020 project, grant agreement No 654000. We would also like to thank Dr. Sarah Morgan at the University of Southern Mississippi for the use of the Advanced Rheometric Expansion System (ARES-LS).

References

1. Xu, J. *et al.* Highly stretchable polymer semiconductor films through the nanoconfinement effect. *Science (80-.).* **355**, 59–64 (2017).
2. Wang, S. *et al.* Skin electronics from scalable fabrication of an intrinsically stretchable transistor array. *Nature* **555**, 83–88 (2018).
3. Inal, S., Rivnay, J., Suiu, A. O., Malliaras, G. G. & McCulloch, I. Conjugated Polymers in Bioelectronics. *Acc. Chem. Res.* **51**, 1368–1376 (2018).
4. Himmelberger, S. & Salleo, A. Engineering semiconducting polymers for efficient charge transport. *MRS Commun.* **5**, 383–395 (2015).
5. Müller, C. On the glass transition of polymer semiconductors and its impact on polymer solar cell stability. *Chem. Mater.* **27**, 2740–2754 (2015).
6. Savagatrup, S., Makaram, A. S., Burke, D. J. & Lipomi, D. J. Mechanical properties of conjugated polymers and polymer-fullerene composites as a function of molecular structure. *Adv. Funct. Mater.* **24**, 1169–1181 (2014).
7. Sugiyama, F. *et al.* Effects of flexibility and branching of side chains on the mechanical properties of low-bandgap conjugated polymers. *Polym. Chem.* 4354–4363 (2018). doi:10.1039/C8PY00820E
8. AIME, J. P., BARGAIN, F. & Schott, M. Structural Study of Conducting Polymers in Solution. *Synth. Met.* **28**, C407–C417 (1989).
9. Yamamoto, T. *et al.* Extensive studies on π-stacking of poly(3-alkylthiophene-2,5-diyl)s and poly(4-alkylthiazole-2,5-diyl)s by optical spectroscopy, NMR analysis, light scattering analysis, and X-ray crystallography. *J. Am. Chem. Soc.* **120**, 2047–2058 (1998).
10. McCulloch, B. *et al.* Polymer Chain Shape of Poly(3-alkylthiophenes) in Solution Using Small-Angle Neutron Scattering. *Macromolcules* **45**, (2013).
11. Fytas, G., Nothofer, H. G., Scherf, U., Vlassopoulos, D. & Meier, G. Structure and dynamics of nondilute polyfluorene solutions. *Macromolecules* **35**, 481–488 (2002).
12. Gettinger, C. L., Heeger, A. J., Drake, J. M. & Pine, D. J. A photoluminescence study of poly(phenylene vinylene) derivatives: The effect of intrinsic persistence length. *J. Chem. Phys.* **101**, 1673–1678 (1994).
13. Kuei, B. & Gomez, E. D. Chain conformations and phase behavior of conjugated polymers. *Soft Matter* **13**, 49–67 (2017).
14. Roth, B. *et al.* Mechanical Properties of a Library of Low-Band-Gap Polymers. *Chem. Mater.* **28**, 2363–2373 (2016).
15. Zhang, S. *et al.* The Critical Role of Electron-Donating Thiophene Groups on the Mechanical and Thermal Properties of Donor–Acceptor Semiconducting Polymers. *Adv. Electron. Mater.* **5**, 1800899 (2019).
16. Gasperini, A., Bivaud, S. & Sivula, K. Controlling conjugated polymer morphology and charge carrier transport with a flexible-linker approach. *Chem. Sci.* **5**, 4922–4927 (2014).
17. Savagatrup, S., Zhao, X., Chan, E., Mei, J. & Lipomi, D. J. Effect of Broken Conjugation on the Stretchability of Semiconducting Polymers. *Macromol. Rapid Commun.* **37**, 1623–1628 (2016).
18. Zhao, X. *et al.* Complementary Semiconducting Polymer Blends: The Influence of Conjugation-Break Spacer Length in Matrix Polymers. *Macromolecules* **49**, 2601–2608 (2016).
19. Zhao, Y. *et al.* Conjugation-break spacers in semiconducting polymers: Impact on polymer processability and charge transport properties. *Macromolecules* **48**, 2048–2053 (2015).
20. Schroeder, B. C. *et al.* Non-Conjugated Flexible Linkers in Semiconducting Polymers: A Pathway to Improved Processability without Compromising Device Performance. *Adv. Electron. Mater.* **2**, (2016).

21. Zhao, Y. *et al.* Melt-Processing of Complementary Semiconducting Polymer Blends for High Performance Organic Transistors. *Adv. Mater.* **29**, 1–7 (2017).
22. Wang, G. J. N. *et al.* Nonhalogenated Solvent Processable and Printable High-Performance Polymer Semiconductor Enabled by Isomeric Nonconjugated Flexible Linkers. *Macromolecules* **51**, 4976–4985 (2018).
23. Oh, J. Y. *et al.* Intrinsically stretchable and healable semiconducting polymer for organic transistors. *Nature* **539**, 411–415 (2016).
24. Melenbrink, E. L. *et al.* Influence of Systematic Incorporation of Conjugation-Break Spacers into Semi-Random Polymers on Mechanical and Electronic Properties. *ACS Appl. Mater. Interfaces* **10**, 32426–32434 (2018).
25. Melenbrink, E. L. *et al.* Influence of Acceptor Side-Chain Length and Conjugation-Break Spacer Content on the Mechanical and Electronic Properties of Semi-Random Polymers. *ACS Appl. Polym. Mater.* **1**, 1107–1117 (2019).
26. Printz, A. D., Savagatrup, S., Burke, D. J., Purdy, T. N. & Lipomi, D. J. Increased elasticity of a low-bandgap conjugated copolymer by random segmentation for mechanically robust solar cells. *RSC Adv.* **4**, 13635–13643 (2014).
27. Kim, J. S. *et al.* Tuning Mechanical and Optoelectrical Properties of Poly(3-hexylthiophene) through Systematic Regioregularity Control. *Macromolecules* **48**, 4339–4346 (2015).
28. Son, S. Y. *et al.* High-Field-Effect Mobility of Low-Crystallinity Conjugated Polymers with Localized Aggregates. *J. Am. Chem. Soc.* **138**, 8096–8103 (2016).
29. SasView. (2019). Available at: www.sasview.org.
30. Qian, Z. *et al.* Challenge and Solution of Characterizing Glass Transition Temperature for Conjugated Polymers by Differential Scanning Calorimetry. *J. Polym. Sci. Part B Polym. Phys.* **57**, 1635–1644 (2019).
31. Qian, Z. *et al.* Glass Transition Phenomenon for Conjugated Polymers. *Macromol. Chem. Phys.* **220**, (2019).
32. Sharma, A., Pan, X., Campbell, J. A., Andersson, M. R. & Lewis, D. A. Unravelling the Thermomechanical Properties of Bulk Heterojunction Blends in Polymer Solar Cells. *Macromolecules* **50**, 3347–3354 (2017).
33. Zhang, S. *et al.* Probing the Viscoelastic Property of Pseudo Free-Standing Conjugated Polymeric Thin Films. *Macromol. Rapid Commun.* **39**, 1800092 (2018).
34. Wang, G.-J. N. *et al.* Tuning the Cross-Linker Crystallinity of a Stretchable Polymer Semiconductor. *Chem. Mater.* **31**, 6465–6475 (2019).
35. Ocheje, M. U. *et al.* Influence of amide-containing side chains on the mechanical properties of diketopyrrolopyrrole-based polymers. *Polym. Chem.* **9**, 5531–5542 (2018).
36. Lin, B. *et al.* Molecular packing control enables excellent performance and mechanical property of blade-cast all-polymer solar cells. *Nano Energy* **59**, 277–284 (2019).
37. Tummala, N. R., Risko, C., Bruner, C., Dauskardt, R. H. & Brédas, J. L. Entanglements in P3HT and their influence on thin-film mechanical properties: Insights from molecular dynamics simulations. *J. Polym. Sci. Part B Polym. Phys.* **53**, 934–942 (2015).
38. Koch, F. P. V. *et al.* The impact of molecular weight on microstructure and charge transport in semicrystalline polymer semiconductors–poly(3-hexylthiophene), a model study. *Prog. Polym. Sci.* **38**, 1978–1989 (2013).
39. Balar, N. *et al.* The Importance of Entanglements in Optimizing the Mechanical and Electrical Performance of All-Polymer Solar Cells. *Chem. Mater.* **31**, 5124–5132 (2019).
40. Xie, R. *et al.* Glass Transition Temperature of Conjugated Polymers by Oscillatory Shear Rheometry. *Macromolecules* **50**, 5146–5154 (2017).
41. Xie, R., Colby, R. H. & Gomez, E. D. Connecting the Mechanical and Conductive Properties of Conjugated Polymers. *Adv. Electron. Mater.* **4**, (2018).
42. Xie, R. *et al.* Local Chain Alignment via Nematic Ordering Reduces Chain Entanglement in Conjugated Polymers. *Macromolecules* **51**, 10271–10284 (2018).
43. Costanzo, S., Pasquino, R., Läuger, J. & Grizzuti, N. Milligram Size Rheology of Molten Polymers. *Fluids* **4**, 28 (2019).
44. van Gurp, M. & Palmen, J. Time-temperature superposition for polymeric blends. *J Rheol Bull* **65**, 5–8 (1998).
45. Trinkle, S. VanGurp-Palmen-plot. *Rheol. Acta* **40**, 322–328 (2001).
46. Qian, Z. *et al.* Linear Rheology of a Series of Second-Generation Dendronized Wedge Polymers. *Macromolecules* **52**, 2063–2074 (2019).
47. Ferry, J. . *Viscoelastic Properties of Polymers. 3rd ed.* (John Wiley & Sons, Inc., 1980).
48. Brinkmann, M. *et al.* Segregated versus mixed interchain stacking in highly oriented films of naphthalene diimide bithiophene copolymers. *ACS Nano* **6**, 10319–10326 (2012).
49. Takacs, C. J. *et al.* Remarkable order of a high-performance polymer. *Nano Lett.* **13**, 2522–2527 (2013).
50. Walker, L. M. & Wagner, N. J. SANS Analysis of the Molecular Order in Poly(γ-benzyl. *Society* 2298–2301 (1996).
51. Gurau, M. C. *et al.* Measuring molecular order in poly(3-alkylthiophene) thin films with polarizing spectroscopies. *Langmuir* **23**, 834–842 (2007).
52. Pedersen, J. S. & Schurtenberger, P. Scattering functions of semiflexible polymers with and without excluded volume effects. *Macromolecules* **29**, 7602–7612 (1996).